



HAL
open science

The astrophysical context of collision processes in meteorites

Yves Marrocchi, Marco Delbo, Matthieu Gounelle

► **To cite this version:**

Yves Marrocchi, Marco Delbo, Matthieu Gounelle. The astrophysical context of collision processes in meteorites. *Meteoritics and Planetary Science*, 2021, 56 (7), pp.1406-1421. 10.1111/MAPS.13716 . hal-03368924

HAL Id: hal-03368924

<https://hal.science/hal-03368924>

Submitted on 7 Oct 2021

HAL is a multi-disciplinary open access archive for the deposit and dissemination of scientific research documents, whether they are published or not. The documents may come from teaching and research institutions in France or abroad, or from public or private research centers.

L'archive ouverte pluridisciplinaire **HAL**, est destinée au dépôt et à la diffusion de documents scientifiques de niveau recherche, publiés ou non, émanant des établissements d'enseignement et de recherche français ou étrangers, des laboratoires publics ou privés.

The astrophysical context of collision processes in meteorites

Yves Marrocchi^{1,*}, Marco Delbo² & Matthieu Gounelle³

¹Université de Lorraine, CNRS, Centre de Recherches Pétrographiques et Géochimiques (CRPG), UMR 7358, Vandoeuvre les Nancy, F-54501, France

²Université Côte d'Azur, Observatoire de la Côte d'Azur, CNRS, Laboratoire Lagrange, CS 34229, 06304 Nice, France

³IMPMC, Muséum national d'Histoire naturelle, Sorbonne Universités, CNRS, UMR 7590, 57 rue Cuvier, 75005 Paris, France

*Corresponding author: yvesm@crpg.cnrs-nancy.fr

Abstract

Chondrites are leftover solids from the early evolution of the solar protoplanetary disk that never experienced melting since their formation. They comprise unequilibrated assemblages of low- and high-temperature components, including volatile-rich, fine-grained matrices, Fe-Ni metal, [sulfides](#), refractory inclusions, and chondrules. Consequently, chondrites are commonly described as *pristine*, *primitive*, or *primordial* rocks of the solar system. However, impact-generated secondary features are abundant in chondrites, suggesting that collisions among early-formed planetesimals and their fragmentation and reassembly have been effective throughout the evolution of the solar system. In this report, we review evidence of the major role of impacts in generating the current mineralogical and petrographic characteristics of chondrites. We provide perspective to these meteoritic features by discussing recent analyses of large-scale structures of the main asteroid belt and remote-sensing observations of asteroids. Observations at various spatial scales all attest [that](#) the 'primitive' materials formed during the evolution of the solar system have largely been

32 reprocessed, confirming previous studies that primitivity is relative, not absolute. This implies
33 that (i) chondrites (and some differentiated meteorites) should systematically be envisioned as
34 reprocessed and heterogeneous materials and (ii) brecciated meteorites should be considered
35 the norm and unbrecciated meteorites the exception.

36

37

38 **Keywords:** chondrites, clasts, brecciation, asteroids, impacts

39

40

41

42

43

44

45

46

47

48

49

50

51

52

53

54

55 **1- Introduction**

56

57 Meteorites are asteroidal (or rarely cometary; Gounelle et al. 2006) fragments
58 recovered at the Earth's surface either promptly after their falls (e.g., Hiroi et al., 2001;
59 Jenniskens et al. 2012; Marrocchi et al. 2020) or during field trips to cold/hot deserts (e.g.,
60 [Bischoff and Geiger 1995](#); [Evatt et al. 2020](#); [Gattacceca et al. 2011](#); [Harvey 2003](#); [Schlüter et](#)
61 [al. 2002](#)). Meteorites' parent bodies are leftovers from the planetary formation processes that
62 operated during the evolution of the solar system. Differentiated parent bodies recorded
63 processes such as metal-silicate differentiation, early volcanism, [granite-like magmatism](#) and
64 magma ocean episodes (e.g., [Bischoff et al. 2014](#); [Terada and Bischoff, 2009](#)). In contrast,
65 chondritic parent bodies did not experience melting and comprise high-temperature
66 components formed in the solar protoplanetary disk (SPD) before planetesimal accretion,
67 namely refractory inclusions (Ca-Al-rich inclusions, CAIs, and amoeboid olivine aggregates,
68 AOA; e.g., [Marrocchi et al. 2019a](#)) and chondrules (e.g., [Connolly and Jones 2016](#)).
69 Chondrites thus represent invaluable witnesses of the SPD's evolution because they are made
70 of components that formed at different times and locations in the SPD ([Bollard et al. 2019](#);
71 [Connelly et al. 2012](#); [Kawasaki et al. 2019](#); [MacPherson et al. 2012](#); [Pape et al. 2019](#); [Petitat](#)
72 [et al. 2011](#); [Villeneuve et al. 2009](#)).

73 However, most chondrites experienced subsequent thermal and hydrothermal
74 alteration during asteroidal evolution, which blurred their initial textures, mineralogies, and
75 chemical and isotopic compositions ([Amsellem et al. 2020](#); [Brearley 2006](#); [Fujiya et al. 2015](#);
76 [Huss et al. 2006](#); [Marrocchi et al. 2018a, 2021](#); [Turner et al. 2021](#); [Vacher et al. 2017, 2019a,](#)
77 [2019b, 2020](#)). Based on these modifications, chondrites are assigned petrologic types on a
78 scale from 1 to 6, reflecting the progressive roles of low-temperature aqueous alteration (from
79 type 3 to 1) and thermal metamorphism (from type 3 to 6; [van Schmus and Wood, 1967](#)).

80 Type-3 chondrites thus correspond to materials that underwent minimal modifications after
81 their agglomeration. Despite having suffered hydrothermal alteration of varying intensity,
82 high-temperature components in type-2 chondrites are thought to preserve evidence of the
83 conditions of dust formation in the SPD (e.g., Chaumard et al. 2018; Kööp et al. 2016;
84 Marrocchi et al. 2018b, 2019b; Piani et al., 2021). Consequently, these peculiar chondrites are
85 commonly described as *pristine*, *primitive*, or *primordial* rocks of the solar system (Gounelle
86 2011; Libourel et al. 2017).

87 In addition to secondary alteration processes, hypervelocity impacts are of
88 fundamental importance and played a key role in the early solar system and during its
89 evolution (Bischoff et al., 2021; Raymond and Morbidelli 2020), yet have often been
90 overlooked or treated in unrelated contexts (e.g., Lauretta and McSween 2006). The classical
91 model of planetary formation involves three main steps, all entailing collisional processes. In
92 the first, dust particles experience low-velocity collisions while migrating toward the disk's
93 midplane, thus forming fractal aggregates that subsequently form pebbles through collision-
94 induced compaction (Blum and Wurm 2008; Johansen et al. 2007). The second step is
95 characterized by the collision-induced coagulation of planetesimals, which forms massive
96 planetary embryos and cores (Morbidelli et al. 2016). In the third step, gravitational
97 instabilities induce collisions between planetary embryos, forming terrestrial planets on a time
98 scale of 10^7 – 10^8 years (Raymond and Morbidelli 2020; Raymond et al. 2009). Furthermore,
99 the Moon, whose presence next to the Earth has shaped its evolution, is the result of a giant
100 impact within the first 100 million years of the formation of CAIs (Canup 2012; Canup and
101 Asphaug 2001). Fundamentally, all steps of planetary formation involve collisional processes,
102 implying that they played a key role in shaping the present architecture of the solar system
103 and that they are not an epiphenomenon that can be treated independently of other processes.

104 Collisions have occurred continually through the present and are now the main factor
105 driving the evolution of the asteroid belt, planetary and moon surfaces, and the formation and
106 sustainability of Saturn's rings (Crida and Charnoz 2012). This is exemplified by the complex
107 structures of boulders on near-Earth asteroids (101955) Bennu and (162173) Ryugu, as
108 recently revealed by high-spatial-resolution images obtained by NASA's and JAXA's sample
109 return missions OSIRIS-REx and Hayabusa2, respectively (DellaGiustina et al. 2019;
110 Jaumann et al. 2019; Lauretta et al. 2019a, 2019b; Sugita et al. 2019). In particular, the
111 discovery of craters in the surfaces of Bennu's boulders revealed the effects of meteoroid
112 impacts on this asteroid, which occurred only in the last 1.75 Myr (Ballouz et al. 2020).
113 Furthermore, recent analyses of the main asteroid belt have revealed that only a very limited
114 number of the asteroids that we catalogue today have survived intact from primordial times
115 (Delbo et al. 2017), whereas the large majority of asteroids are fragments (Dermott et al.
116 2018) that experienced disruption of their parent bodies and re-accumulation (Michel 2001;
117 Michel and Richardson 2013; Michel et al. 2020). In this report, we thus aim to (i) detail the
118 astrophysical context of collisional processes in meteorites and (ii) put recent astrophysical
119 and planetological observations in a chondritic perspective.

120

121 **2- Meteoritic evidence of widespread collision processes in the asteroid belt**

122

123 Asteroidal collisions represent a major evolutionary process for solid bodies in the
124 solar system and have played a key role in establishing chondritic features, even in the
125 putative 'primitive' type-2 and -3 chondrites. This is attested by the ubiquitous occurrence of
126 brecciated textures in meteorites, with ~30% of ordinary chondrites (OCs) and almost all CM
127 carbonaceous chondrites showing brecciation features (Fig. 1A; Bischoff et al. 1998; 2006;
128 Gattacceca et al. 2017; Lentfort et al., 2021; Suttle et al., 2021). Such characteristics are

129 fundamental because (i) OCs are by far the most common meteorites falling on Earth (~80%)
130 and (ii) CMs represent 25% of all carbonaceous chondrite falls (Gounelle et al. 2005). Even
131 rarer chondrite types like CI carbonaceous chondrites (Alfing et al. 2019), Rumuruti
132 chondrites (Bischoff et al. 2011), C1 chondrites (Bischoff et al., 2021), CB/CH chondrites
133 (Briani et al., 2009; Bonal et al., 2010), and enstatite chondrites (Fig. 1B; Piani et al., 2016,
134 2020) have brecciated textures, thus implying that all chondrite types have been reprocessed
135 after the accretion of their respective parent bodies.

136 Different types of brecciation are commonly observed among meteorites, revealing
137 that collision and re-agglomeration processes occurred at varying scales and intensities
138 (Bischoff et al. 2006; Rubin 1983). *Monomict breccias* are the most common and correspond
139 to meteorites formed by the *in situ* progressive fracturing and compaction of a single lithology
140 at a scale much smaller than their asteroidal parent bodies. *Impact-melt breccias* (Fig. 1B) are
141 rocks in which the matrix cementing the brecciated fragments crystallized from impact-
142 generated melts. *Genomict breccias* define meteorites containing fragments of the same
143 compositional group, but with different metamorphic or hydrothermal alteration histories
144 (Fig. 2; Gattacceca et al. 2017; Vacher et al. 2018; Verdier-Paoletti et al. 2019; Stöffler et al.,
145 2018); these textures reflect large-scale brecciation processes occurring within a given parent
146 body. In contrast, *polymict breccias* define meteorites composed of fragments originating
147 from different parent bodies (Fig. 3; Bischoff et al. 2006; Zolensky and Ivanov 2003); these
148 are of fundamental importance as they (i) record asteroidal mixing processes and (ii) contain
149 unique clasts not observed as individual samples (Patzek et al. 2018, 2020). The violent
150 evolution of the solar system is also evidenced by commonly observed petrofabrics and/or
151 flattened chondrules and refractory inclusions (Fig. 4; Gattacceca et al. 2005; Greashake
152 2014; Hanna et al. 2015; Rubin 2012; Vacher et al. 2018), which are generally interpreted to
153 result from impact-induced preferential orientations.

154 Furthermore, all classes of meteorites contain xenolith clasts (Fig. 5)—characterized
155 by different lithologies than their respective host rocks (e.g., Bischoff et al. 2006; Bonal et al.
156 2010; Briani et al. 2009, 2012; Liu et al. 2020; Patzek et al. 2020; Zolensky et al. 1996)—
157 resulting from the low-velocity incorporation (i.e., $<1 \text{ km s}^{-1}$; Briani et al. 2011) of
158 micrometeoroids by asteroidal parent bodies (Briani et al. 2011; Rubin and Bottke 2009).
159 Such clasts differ from polymict breccias because they could have been incorporated into
160 asteroids throughout the evolution of the solar system. The mixing of the host and xenoliths
161 probably at low-velocity is also attested by the lack of thermal metamorphism between the
162 clasts and their host meteorites (Fig. 6). Interestingly, the very few occurrences of CC clasts
163 in OC chondrites could result from the fragile nature of carbonaceous materials relative to
164 their OC counterparts. Taken together, brecciated textures, xenolith clasts, and petrofabrics
165 thus all attest to the violent evolution of the solar system, both during the first ~5–10 Myr of
166 the SPD's evolution and continuing today.

167 Finally, the presence of high-pressure minerals in most meteorite groups is strong
168 evidence of pervasive impacts on their parent bodies. Indeed, most of these minerals have
169 been found within or adjacent to dark shock veins. Following the discovery of ringwoodite—
170 the spinel-structured polymorph of olivine—in Tenham, a large variety of shock-induced
171 minerals have been discovered, including majorite, akimotoite (the ilmenite-structured
172 polymorph of MgSiO_3), and plagioclase with the hollandite structure (Sharp and DeCarli,
173 2006). At present, high-pressure minerals are used to constrain the pressures, temperatures,
174 and timescales of collision-induced shocks.

175

176 **3- The chaotic origin of the main asteroid belt**

177

178 The first step of asteroid formation occurred ~4.56 Ga when dust grains within the
179 protoplanetary disk surrounding the Sun accreted to form rocky/icy planetesimals ~100 km in

180 diameter. These were the first solid objects in the solar system whose internal strengths were
181 dominated by self-gravity (Johansen et al. 2007; Klahr and Schreiber 2020; Marcus 1967;
182 Morbidelli and Raymond 2016; Safronov and Zvjagina 1969). Although these objects
183 represent the main building blocks of terrestrial planets and the cores of giant planets, their
184 formation conditions and initial size distribution remain a matter of debate (Klahr and
185 Schreiber 2020). Classical models are based on the bottom-up progressive coagulation of
186 small solids into planets via merging collisions. However, during the disk's evolution, such
187 bottom-up planetesimal accretion is fundamentally limited by the 'meter-sized barrier': meter-
188 sized planetesimals will experience (i) rapid drift toward the central star and associated
189 evaporation and (ii) destruction during high-speed collisions (Wetherill 1990; Wurm et al.
190 2005). Recent models thus suggest that planetesimals were initially large (100–1,000 km) due
191 to high concentrations of small solid particles in turbulent structures of the SPD (Cuzzi et al.
192 2008; Johansen et al. 2007; Morbidelli et al. 2009). Such models are in agreement with
193 studies reconstructing the size distribution of planetesimals from analyses of the current
194 asteroid population (Bottke et al. 2005; Delbo et al. 2017, 2019; Morbidelli et al. 2009;
195 Tsirvoulis et al. 2018). However, most known asteroids are much smaller than planetesimals
196 (Masiero et al. 2014), indicating that they are remnants produced by the collisional
197 fragmentation of larger parent bodies, including planetesimals, throughout the history of the
198 solar system. An investigation of the dynamical behavior of asteroids reached the same
199 conclusion (Dermott et al. 2018). These results imply that (i) the current asteroid population is
200 the result of a dramatic collisional evolution that must also be reflected in the physical and
201 textural properties of meteorites and (ii) similar to meteorites, the current architecture of
202 asteroid belt [cannot be considered](#) as a direct witness of the early solar system.

203 [Most of planetesimal collisions have occurred in the main asteroid belt, between the](#)
204 [orbits of Mars and Jupiter \(heliocentric distances of ~2–3.2 AU\), where most known asteroids](#)

205 are currently located. Contrary to common perceptions, the main belt is mostly empty,
206 containing only 5×10^{-4} Earth masses (i.e., ~4 % of the mass of the Moon), with asteroids
207 spread over an annular area more than three times as wide as the distance between Mercury
208 and Mars. In addition, about half of the main-belt mass is contained in the four largest
209 asteroids: Ceres, Vesta, Pallas, and Hygiea (DeMeo and Carry 2014). The main belt is
210 dynamically excited, with orbital eccentricities (e) up to 0.3 and inclinations (i) of 0 to $>20^\circ$,
211 and is characterized by the presence of spectroscopically distinct asteroids that, in general,
212 correspond to distinct compositions (Fig. 7; Bus and Binzel 2002a, 2002b; DeMeo and Carry
213 2014): C-type asteroids are water-rich and genetically linked to carbonaceous chondrites,
214 whereas S-type asteroids are dry and related to OCs. The compositions of asteroids vary as a
215 function of their orbital semimajor axis (a): S-type asteroids are more abundant in the inner
216 and central main belt ($2.1 < a < 2.7$ AU) whereas C-type asteroids are more abundant in the
217 outer regions ($2.7 < a < 3.2$ AU).

218 Since the discovery of the first asteroids in the early nineteenth century, the main belt
219 was long considered to be a ‘living relic’ of planetary formation. Canonical planetary
220 formation theories postulated that (i) asteroids remained at the heliocentric distances at which
221 they formed (as for planetesimals; Gradie and Tedesco 1982) and (ii) the compositional
222 gradient of the main belt reflects that of the SPD from the inner border of the protoplanetary
223 disk (a few tenths of an AU from the Sun) out to Jupiter (Raymond et al. 2006). However,
224 these views began to shift in the mid-2000s. First, it was proposed that iron-meteorite parent
225 bodies could have formed in the region of terrestrial planets before being scattered to the main
226 belt by gravitational interactions with the growing terrestrial protoplanets (Bottke et al. 2006).
227 Second, dynamic models suggested that the D-type asteroids observed today in the main belt
228 are not indigenous, but instead correspond to trans-Neptunian objects that were scattered into
229 the main belt by the giant planets during their instability phase (Fujiya et al. 2019; Levison et

230 al. 2009; Marrocchi and Piani 2019; Morbidelli et al. 2010; Tsiganis et al. 2005). Following
231 these pioneering works, main-belt asteroid implantation models were advanced using new
232 dynamic models involving giant-planet formation and migration early in the solar system.
233 These models were developed to address two principle stumbling blocks of the classical
234 ‘static’ models: they systematically produce (i) Mars analogs as massive as the Earth, rather
235 than about a tenth of the Earth’s mass, and (ii) eccentricity and inclination distributions of
236 asteroids that do not match those of the current belt. Although important uncertainties remain,
237 the following three recent models (Fig. 7) have successfully reproduced these peculiar
238 characteristics and suggest that the entire main belt population of dynamically excited and
239 radially mixed S- and C-type asteroids are not indigenous, but were implanted in their current
240 locations between the terrestrial- and giant-planet regions.

241

242 **(i) The “grand tack” model** proposed that the inward and subsequent outward migrations of
243 Jupiter and Saturn in the protoplanetary disk truncated the disk at 1 AU, limiting the material
244 available for the formation of Mars (Fig. 7; Walsh et al. 2011). In this scenario, an initial
245 population of planetesimals was expelled from the main belt by the inward migration of
246 Jupiter, which plunged through the main belt. The main belt was subsequently repopulated by
247 planetesimals during the outward migration of Jupiter (Walsh et al. 2011). In this scenario,
248 planetesimals suffered mutual collisions at velocities $> 10 \text{ km s}^{-1}$ (Johnson et al. 2016).

249

250 **(ii) The low-mass asteroid belt model** preserves the concept of implanting planetesimals
251 into the main belt from the terrestrial- (S-types) and giant-planet regions (C-types; Raymond
252 and Izidoro 2017a, 2017b). However, contrary to other models such as the grand tack model,
253 these authors showed that the main belt could have initially had a low mass (or could have
254 even been empty) and that large-scale migrations of the giant planets are not required to

255 populate it with the current mixture of asteroid types (Fig. 7). In this model, C- and S-type
256 asteroids were implanted not only from different sources but also at different times: C-type
257 planetesimals that formed in the giant-planet region were scattered inward during the gas
258 phase of the protoplanetary disk (i.e., within a few million years after the formation of CAIs;
259 Raymond and Izidoro 2017a, 2017b), whereas S-type asteroids were implanted from the
260 terrestrial-planet region into the main belt after the gas in the protoplanetary disk had
261 dissipated (i.e., later than ~10 Myr after the formation of CAIs). The implantation of S-type
262 asteroids was slower and more prolonged than that of C-type asteroids, possibly lasting 100
263 Myr (Raymond and Izidoro 2017b) because, in this model, S-type planetesimals must have
264 been scattered via multiple close encounters with planetary embryos. In such models, Mars'
265 small mass results from a primordial mass deficit between the present-day orbits of Earth and
266 Jupiter (Hansen 2009).

267

268 **(iii) The early instability model** recently provided an alternative view in which the giant
269 planets did not undergo large migrations during the gas phase (Fig. 7; Clement et al. 2018,
270 2019a, 2019b). In this model, as in the canonical scenario, a sea of planetesimals spanning the
271 inner rim of the protoplanetary disk (out to Jupiter) was perturbed by an early orbital
272 instability of the giant planets around 10 Myr after gas dispersal, which triggered the
273 formation of the terrestrial planets. This instability also removed significant mass from the
274 main-belt region and broadened the ranges of the eccentricities and inclinations of main-belt
275 planetesimals to the current values, thereby starting the violent collisional evolution of these
276 bodies.

277

278 Although the current orbital structure (semi-major axis, eccentricity, inclination) of the
279 asteroid belt is consistent with an initially uniform distribution of asteroids (Minton and

280 Malhotra 2009), its self-excitation requires several orders of magnitude more mass than is
281 present today (e.g., O'Brien and Sykes 2011). This implies that the belt experienced violent
282 processes that considerably modified its initial structure. Whatever the process that
283 dominantly shaped the asteroid belt, collisional processes were important and common during
284 the early evolution of the solar system. Depending on the scenario invoked, the main belt
285 reached its current dynamic configuration after tens to hundreds of millions of years (e.g.,
286 after giant-planet instability). Since then, collisions have continued to occur with typical
287 impact velocities between asteroids of $\sim 5.3 \text{ km s}^{-1}$ (Bottke et al. 2005 and references therein),
288 although the impact velocities define a broad distribution and collisions at higher-than-
289 average speeds are not uncommon, particularly for objects with high i and/or e values. One
290 such case is the [third-largest](#) asteroid (2) Pallas ($i = 34.8^\circ$, $e = 0.23$), for which impact
291 [velocities are estimated to be \$\sim 12 \text{ km s}^{-1}\$ on average](#) (Marsset et al. 2020). Collisions at such
292 speeds can yield temperatures high enough to induce the dehydration and thermal
293 metamorphism of asteroidal materials, which should be observable in the meteorites that we
294 may receive from these bodies (Amsellem et al. 2020 and references therein). This collisional
295 evolution is responsible for the formation of the families of asteroid fragments (Nesvorny et
296 al. 2015) that we observe in the main belt. The effects of these collisions, which can lead to
297 the mixing of asteroidal materials of different compositions, is also visible in some physical
298 properties of asteroids, as it is detailed in the next section.

299

300 **4- Evidence for collisional processes from *in-situ* exploration of asteroids**

301

302 [In situ](#) exploration by space missions and telescopic observations of asteroids provide
303 [growing evidence of the effects of impacts and the resulting material mixing produced by the](#)
304 [infall of exogenic impacting objects.](#)

305 The first evidence of the violent collisional evolution of asteroids is the presence of
306 craters on their surfaces. This has been clear since NASA's Galileo mission, the first
307 spacecraft to fly by an asteroid, which imaged (951) Gaspra in 1991 (Veverka et al. 1994) and
308 showed that its surface is covered by impact craters (Stooke 1996). Since then, impact craters
309 appear to be ubiquitous structures as they have been observed on all imaged asteroids. These
310 craters range in size from the ~500-km-diameter Rheasilvia basin near the south pole of (4)
311 Vesta (Schenk et al. 2012; Thomas et al. 1997) to decimeter-scale craters in boulders on the
312 surface of the 500-m-diameter near-Earth asteroid (101955) Bennu (Ballouz et al. 2020). On
313 Vesta, the deposition of the so-called 'dark material' that is often associated with craters has
314 been attributed to impacts by carbonaceous asteroids (McCord et al. 2012). This dark material
315 is then (i) diffused throughout the regolith of the surface of Vesta over time (McCord et al.
316 2012) and (ii) compressed by subsequent impacts on the surface and cemented together with
317 original Vestan material (brighter in color) into breccia-like rocks. This process is in good
318 agreement with the common presence of clasts of carbonaceous chondritic materials within
319 Howardites (e.g., Fig. 5; Buchanan et al., 1993; Liu et al. 2020; McSween et al. 2011; van
320 Drongelen et al., 2016), regolith breccia meteorites belonging to the HED group and
321 originating from the surface of Vesta.

322 Because Vesta is a differentiated asteroid, it has been proposed that impacts could
323 excavate its basaltic crust, revealing its underlying olivine mantle. However, very little olivine
324 has been detected at Vesta's surface, even in and around the giant impact basins Rheasilvia
325 and Venenia (Ammannito et al. 2013; De Sanctis et al. 2012). Therefore, the rare occurrences
326 of olivine signatures on Vesta's surface may rather correspond to material implanted by
327 olivine-rich impactors (Turrini et al. 2016). Indeed, laboratory impact experiments performed
328 at velocities similar to the average impact velocity on Vesta demonstrated that impactor
329 material could be preserved at Vesta's surface (Daly and Schultz 2016). Although the

330 survivability and implantation of impactor material is a function of impact velocity,
331 laboratory hypervelocity impact experiments on porous and non-porous targets showed that
332 impact-generated material implantation is a general process occurring throughout the solar
333 system (Avdellidou et al. 2016, 2017). This implies that the mixing of asteroidal materials
334 was possible not only during the early gas phase of the SPD when impact velocities were
335 lower, but throughout the history of the solar system. Interestingly, high-speed collisions (i.e.,
336 12 km s^{-1} ; Marsset et al. 2020) can also yield temperatures high enough to induce the
337 dehydration and thermal metamorphism of asteroidal materials (Amsellem et al. 2020 and
338 references therein).

339 Very recent observations at cm-scale spatial resolution of the surfaces of the near-
340 Earth asteroids (101955) Bennu and (162173) Ryugu by NASA's OSIRIS-REx (Lauretta et al.
341 2019a, 2019b) and JAXA's Hayabusa2 (Okada et al. 2020; Tatsumi et al. 2021) sample return
342 missions, respectively, provide a wealth of indications about the mixing of asteroidal
343 materials and the presence of brecciated rocks on these asteroids. OSIRIS-REx spectroscopic
344 and spectrophotometric observations revealed the presence of bright, pyroxene-rich boulders
345 of Vesta-like composition on the dark, carbonaceous surface of Bennu (DellaGiustina et al.
346 2020). This suggests that some asteroids of the Vesta collisional family impacted Bennu, or
347 more likely its parent body, mixing the two materials (DellaGiustina et al. 2020). This is also
348 attested by the peculiar textures of some of Bennu's pyroxene-rich, hummocky boulders,
349 which show potential layering or brecciation (DellaGiustina et al. 2020). Furthermore, two
350 bright, pyroxene-bearing clasts appear embedded within a large, partially buried boulder, the
351 latter having an albedo similar to the average of Bennu (DellaGiustina et al. 2020).
352 Interestingly, the Hayabusa2 orbiter also detected bright material on the dark surface of
353 Ryugu (Tatsumi et al. 2021), thus suggesting that brecciation is a common process during
354 asteroidal evolution.

355 In contrast to Bennu, the spectral signatures of Ryugu indicate two distinct units of
356 bright material. One appears to be more compatible with an S-type asteroidal composition
357 (rather than a pyroxene-rich, Vesta-like nature; Tatsumi et al. 2021) that could have been
358 delivered by an impact (or series of impacts) on Ryugu's parent body. The second unit has
359 spectral features similar to the bulk of Ryugu, but with a less pronounced upturn at ultraviolet
360 frequencies compared to the Ryugu average (Tatsumi et al. 2021). This unit may represent a
361 more thermally metamorphosed material compared to that covering most of the surface of the
362 asteroid (Tatsumi et al. 2021). It thus appears that Ryugu's surface comprises materials
363 originating from various depths within its parent body. Such diverse materials may also be
364 present on other similar asteroids, compacted together by small-scale impacts to form
365 breccias.

366 OSIRIS-REx images of the surface of Bennu show diverse rocks including (i)
367 boulders with albedo and/or color heterogeneities and (ii) non-fractured boulders containing
368 meter-sized clasts (Lauretta et al. 2019a). Such assemblages have been interpreted as impact
369 breccias (e.g., see Fig. 1b of Walsh et al. 2019). However, the collisional processes capable of
370 producing breccia-like boulders several meters in size and containing meter-scale clasts are
371 probably too energetic to be withstood by Bennu itself (Bischoff et al. 2006). Hence, these
372 boulders probably formed on Bennu's parent body and may record (i) the parent body's
373 accretion in the SPD (Walsh et al. 2019), (ii) compaction of regolith blocks on the parent
374 body, or (iii) collisional events that fragmented the parent body to form Bennu. The surfaces
375 of some boulders larger than ten meters in size also appear to be "littered" with brighter
376 centimetric rocks that, in some cases, appear to be cemented together (Bennett et al. 2021).
377 Although the origin of this material is unclear, it may result from (i) impacts on the boulders
378 themselves (Bennett et al. 2021) or (ii) particles falling back onto the asteroid after particle-
379 ejection events, such as were observed on Bennu (Lauretta et al., 2019b).

380 To summarize, the presence of clasts and exogenic components in Bennu and Ryugu
381 imply that material-mixing *via* impacts is a common process on these bodies, and likely
382 throughout the solar system. These observations also give context to what was once a
383 breakthrough in asteroid and meteoritic science, namely the discovery of distinct meteorite
384 classes within the strewn field of the Almahata-Sitta meteorites, which were produced by the
385 atmospheric breakup of asteroid 2008 TC₃ (Bischoff et al. 2010; [Goodrich et al., 2015, 2019;](#)
386 [Horstmann and Bischoff, 2014;](#) Jenniskens et al. 2009). Before the Almahata-Sitta recovery,
387 the canonical concept was that one class of meteorite originates from one class of asteroid.
388 These recent spacecraft observations have thus demonstrated that 2008 TC₃ is perhaps not an
389 exception and that individual asteroids can host materials corresponding to diverse meteorite
390 classes.

391

392 **5- Implications and perspectives**

393

394 Brecciated textures, xenolith clasts, and petrofabrics in meteorites attest to the chaotic
395 evolution of the solar system, both during the first ~5–10 Myr of the evolution of the SPD and
396 continuing until today. Given our knowledge of the structure of the asteroid belt and our
397 theoretical understanding of the evolution of the solar system, this testifies that so-called
398 *primitive materials* formed during the evolution of the SPD have been largely reprocessed,
399 implying that primitivity is relative, not absolute (Bischoff et al. 2019; Gounelle 2011;
400 Libourel et al. 2017). This is not greatly surprising as the spectra of ~20% of nearby solar-
401 type stars of various ages show infrared peaks related to the presence of debris disks, low-
402 mass (i.e., less than the mass of the Earth), low-density, dust-dominated disks that are
403 continuously replenished by collisions between large planetesimals (Hughes et al. 2018).
404 Debris disks are analogous to our solar system's Kuiper Belt and zodiacal light and are

405 fundamentally different from protoplanetary disks, which are dominated by agglomeration
406 processes whereas debris disks are destruction-dominated. This implies that early-formed
407 planetesimals (i) were largely reprocessed during the evolution of the solar system and (ii)
408 experienced fragmentation and subsequent reassembly as asteroids observed today. Indeed,
409 the astronomical survey of the asteroid belt suggests that only a few hundreds of asteroids
410 have remained unchanged since their formation (Delbo et al. 2017), clearly indicating that
411 solar system materials have been largely reprocessed *via* impacts. In addition, planetesimals
412 that accreted during the two million years following CAI formation likely experienced
413 melting due to ^{26}Al decay (Bizzarro et al. 2005; Hevey and Sanders 2006; Sahijpal et al.
414 2007), which, at least partially (i.e., primitive achondrites), erased their primordial features.

415 The complex evolution of asteroids is an ongoing process; recent reports suggest that
416 impact-generated fluid circulations, probably triggered by hypervelocity impacts, have
417 occurred within the past few hundreds of thousands of years (Amsellem et al. 2020; Turner et
418 al. 2021). This is also highlighted by the ubiquitous presence of xenolith clasts in chondrites
419 and achondrites (Bischoff et al. 2006; Bonal et al. 2010; Briani et al. 2009, 2012; Cohen et al.,
420 2004; Liu et al. 2020; Patzek et al. 2018, 2020; Zolensky et al. 1996), which may have been
421 incorporated into their current bodies by implantation processes and/or regolith gardening
422 throughout the evolution of the solar system. Therefore, ‘primitive’ samples are probably
423 extremely rare, and the concept of primitivity should only be used to relatively describe two
424 or several objects, and always in terms of processes.

425 A direct consequence is the limitation of the so-called bulk composition of meteorites,
426 as –depending on the scale sampled– the average composition could have been modified by
427 various processes operating all along the solar system evolution. For example, although CI
428 chondrites are commonly used as a reference for chemical normalization (Lodders 2003), CIs
429 show brecciated structures and are significantly heterogeneous at a scale of just ~100 mg

430 (Morlok et al. 2006) or up to 1 g for elements sensitive to fluid circulation (Barrat et al. 2012).
431 Therefore, virtually all chondrites (and some differentiated meteorites) should be viewed as
432 reprocessed, heterogeneous materials, and analyses of their bulk chemical and isotopic
433 compositions can only provide usable results when specifying the sampling scale. Taken
434 together, all these observations suggest the need for a new perspective on meteorites,
435 considering (i) highly brecciated meteorites (i.e., Kaidun and [Almahata Sitta](#), typically viewed
436 as anomalies) as the norm and (ii) monomict breccias as the exception. In addition, the
437 numerous outstanding questions regarding the origin, distribution, and evolution of xenolith
438 clasts require (i) extensive mineralogical, petrographic, and isotopic characterizations of
439 xenolith clasts (especially in OCs, for which only a limited number have been described), (ii)
440 an understanding of the dynamics and chronology of their incorporation into their host bodies,
441 and (iii) further development of the physics of small-scale implantation processes.

442

443 **Acknowledgments**

444

445 We thank Laurette Piani and Maximilien J. Verdier-Paoletti for providing chondrite
446 pictures. This work is the result of intense scientific discussions during the February 2020
447 workshop “First solids and planetesimals: formation conditions and evolution” hosted in les
448 Houches (France) and organized by the Programme National de Planétologie (PNP). [Nan Liu](#)
449 [and Markus Patzek](#) are warmly thanked for positive and constructive reviews and we thank
450 [Tim Jull](#) for handling the article. This is CRPG contribution #2751.

451

452

453

454

455 **Figure captions**

456

457 **Fig. 1:** A) Reflected-light photograph of a piece of the Boriskino CM chondrite, courtesy of
458 L. D. Bayle. Diverse lithologies, characterized by different shades of gray, are easily
459 distinguished. B) Reflected-light photograph of the enstatite chondrite Abee showing impact-
460 generated veins (Bischoff et al., 2006; Rubin, 2015). Courtesy of Laurette Piani.

461

462 **Fig. 2:** Back-scattered electron image of the brecciated Cold Bokkeveld CM chondrite. In-
463 dividual fragments (some are traced by red dashed lines) are variable in composition, as
464 indicated by their different shades of gray.

465

466 **Fig. 3:** Energy-dispersive X-ray elemental map of the Mg, Al, Si, Ca, and Fe distributions in
467 the polymict breccia Kaidun, revealing its complex nature.

468

469 **Fig. 4:** Back-scattered electron image of CV3 Efremovka, showing a high degree of
470 chondrule flattening induced by hypervelocity impacts. A fine-grained clast is also observed
471 in this section.

472

473 **Fig. 5:** Back-scattered electron images of xenolith clasts (central in each image) observed in
474 (A) CB Isheyev and (B) the Kapoeta Howardite.

475

476 **Fig. 6:** A) Back scattered electron image of the Paris chondrites showing the presence of
477 light-colored clasts (red boxes). B) and C) Back scattered electron images of the contacts
478 between the clasts and the host chondrites. No specific sign of thermal metamorphism is
479 observed.

480 **Fig. 7:** Schematic comparison of the three global models currently proposed for explaining
481 the peculiar structure of the main asteroid belt and the solar system formation (described in
482 section 4).

483

484

485

486

487

488

489

490

491

492

493

494

495

496

497

498

499

500

501

502

503

504

505 **References**

506

- 507 Alfing J., Patzek M., and Bischoff A. 2019. Modal abundances of coarse-grained (>5 µm)
508 components within CI-chondrites and their individual clasts – Mixing of various
509 lithologies on the CI parent body(ies). *Geochemistry* 79:125532.
510
- 511 Ammannito E. et al. 2013. Olivine in an unexpected location on Vesta’s surface. *Nature*
512 504:122–125.
- 513 Amsellem E., Moynier F., Mahan B., and Beck P. 2020. Timing of thermal metamorphism in
514 CM chondrites: Implications for Ryugu and Bennu future sample return. *Icarus*
515 339:113593.
- 516 Avdellidou C., Price M. C., Delbo M., Ioannidis P., and Cole M. J. 2016. Survival of the
517 impactor during hypervelocity collisions – I. An analogue for low porosity targets.
518 *Monthly Notices of the Royal Astronomical Society* 456:2957–2965.
- 519 Avdellidou C., Price M. C., Delbo M., and Cole M. J. 2017. Survival of the impactor during
520 hypervelocity collisions – II. An analogue for high-porosity targets. *Monthly Notices*
521 *of the Royal Astronomical Society* 464:734–738.
- 522 Ballouz R.-L. et al. 2020. Bennu’s near-Earth lifetime of 1.75 million years inferred from
523 craters on its boulders. *Nature* 587:205–209.
- 524 Barrat J. A., Zanda B., Moynier F., Bollinger C., Liorzou C., and Bayon G. 2012.
525 Geochemistry of CI chondrites: Major and trace elements, and Cu and Zn Isotopes.
526 *Geochimica et Cosmochimica Acta* 83:79–92.
- 527 Bennett C. A. et al. 2021. A high-resolution global basemap of (101955) Bennu. *Icarus*
528 357:113690.
- 529 Bischoff A. and Geiger T. 1985. Meteorites from the Sahara: Find locations, shock
530 classification, degree of weathering, and pairing. *Meteoritics* 30, 113-122.
- 531 Bischoff A., Scott E. R. D., Metzler K., and Goodrich C. A. 2006. Nature and origins of
532 meteoritic breccias. In *Meteorites and the early solar system II*, edited by Lauretta D.
533 S. and McSween H. Y. Tucson, Arizona: The University of Arizona Press. pp. 679-
534 712.
- 535 Bischoff A., Horstmann M., Pack A., Laubenstein M., and Haberer S. 2010. Asteroid 2008
536 TC3-Almahata Sitta: A spectacular breccia containing many different ureilitic and
537 chondritic lithologies: Almahata Sitta-A spectacular breccia. *Meteoritics & Planetary*
538 *Science* 45:1638–1656.
- 539 Bischoff A., Vogel N., and Roszjar J. 2011. The Rumuruti chondrite group. *Geochemistry*
540 71:101–133.
- 541 Bischoff A., Horstmann M., Barrat J.-A., Chaussidon M., Pack A., Herwartz D., Ward D.,
542 Vollmer C., and Decker S. 2014. Trachyandesitic volcanism in the early Solar System.
543 *Proceedings of the National Academy of Sciences* 111:12689–12692.

- 544 Bischoff A., Schleiting M., Wieler R., and Patzek M. 2018. Brecciation among 2280 ordinary
545 chondrites – constraints on the evolution of their parent bodies. *Geochimica et*
546 *Cosmochimica Acta* 238, 516-541.
- 547 Bischoff A., Schleiting M., and Patzek M. 2019. Shock stage distribution of 2280 ordinary
548 chondrites—Can bulk chondrites with a shock stage of S6 exist as individual rocks?
549 *Meteoritics & Planetary Science* 54:2189–2202.
- 550 Bischoff A. et al. 2021. The old, unique C1 chondrite Flensburg – Insight into the first
551 processes of aqueous alteration, brecciation, and the diversity of water-bearing parent
552 bodies and lithologies. *Geochimica et Cosmochimica Acta* 293:142–186.
- 553 Bizzarro M., Baker J. A., Haack H., and Lundgaard K. L. 2005. Rapid Timescales for
554 Accretion and Melting of Differentiated Planetesimals Inferred from ²⁶Al-²⁶Mg
555 Chronometry. *ApJ* 632:L41–L44.
- 556 Blum J., and Wurm G. 2008. The Growth Mechanisms of Macroscopic Bodies in
557 Protoplanetary Disks. *Annual Review of Astronomy and Astrophysics* 46:21–56.
- 558 Bollard J. et al. 2019. Combined U-corrected Pb-Pb dating and ²⁶Al-²⁶Mg systematics of
559 individual chondrules – Evidence for a reduced initial abundance of ²⁶Al amongst
560 inner Solar System chondrules. *Geochimica et Cosmochimica Acta* 260:62–83.
- 561 Bonal L., Huss G. R., Krot A. N., and Nagashima K. 2010. Chondritic lithic clasts in the
562 CB/CH-like meteorite Isheyevo: Fragments of previously unsampled parent bodies.
563 *Geochimica et Cosmochimica Acta* 74:2500–2522.
- 564 Bottke W. F., Nesvorný D., Grimm R. E., Morbidelli A., and O’Brien D. P. 2006. Iron
565 meteorites as remnants of planetesimals formed in the terrestrial planet region. *Nature*
566 439:821–824.
- 567 Bottke W.F., Durda D., Nesvorný D., Jedicke R., Morbidelli A., Vokrouhlický D., and
568 Levison H. 2005. The fossilized size distribution of the main asteroid belt. *Icarus*
569 175:111–140.
- 570 Brearley A. J. 2006. The action of water. In *Meteorites and the early solar system II*, edited by
571 Lauretta D. S. and McSween H. Y. Tucson, Arizona: The University of Arizona Press.
572 pp. 587–624.
- 573 Briani G., Gounelle M., Marrocchi Y., Mostefaoui S., Leroux H., Quirico E., and Meibom A.
574 2009. Pristine extraterrestrial material with unprecedented nitrogen isotopic variation.
575 *Proceedings of the National Academy of Sciences of the United States of America*
576 106:10522–10527.
- 577 Briani G., Morbidelli A., Gounelle M., and Nesvorný D. 2011. Evidence for an asteroid-
578 comet continuum from simulations of carbonaceous microxenolith dynamical
579 evolution: Carbonaceous microxenoliths and the asteroid-comet continuum.
580 *Meteoritics & Planetary Science* 46:1863–1877.
- 581 Briani G., Gounelle M., Bourot-Denise M., and Zolensky M. E. 2012. Xenoliths and
582 microxenoliths in H chondrites: Sampling the zodiacal cloud in the asteroid Main Belt.
583 *Meteoritics & Planetary Science* 47:880–902.

- 584 Buchanan P. C., Zolensky M. E. and Reid A. M. 1993. Carbonaceous chondrite clasts in the
585 howardites Bholghati and EET87513. *Meteoritics & Planetary Science* 28: 659-669.
- 586 Bus S.J., and Binzel R.P. 2002a. Phase II of the Small Main-Belt Asteroid Spectroscopic
587 Survey A Feature-Based Taxonomy. *Icarus* 158:146–177.
- 588 Bus S.J., and Binzel R.P. 2002b. Phase II of the Small Main-Belt Asteroid Spectroscopic
589 Survey The Observations. *Icarus* 158:106–145.
- 590 Canup R. M., and Asphaug E. 2001. Origin of the Moon in a giant impact near the end of the
591 Earth’s formation. *Nature* 412:708–712.
- 592 Canup R. M. 2012. Forming a Moon with an Earth-like Composition via a Giant Impact.
593 *Science* 338:1052–1055.
- 594 Chaumard N. I, Defouilloy C., and Kita N. T. 2018. Oxygen isotope systematics of
595 chondrules in the Murchison CM2 chondrite and implications for the CO-CM
596 relationship. *Geochimica et Cosmochimica Acta* 228:220–242.
- 597 Clement M. S., Kaib N. A., Raymond S. N., and Walsh K. J. 2018. Mars’ growth stunted by
598 an early giant planet instability. *Icarus* 311:340–356.
- 599 Clement M. S., Raymond S. N., and Kaib N. A. 2019a. Excitation and Depletion of the
600 Asteroid Belt in the Early Instability Scenario. *The Astronomical Journal* 157:38.
- 601 Clement M. S., Kaib N. A., Raymond S. N., Chambers J. E., and Walsh K. J. 2019b. The
602 early instability scenario: Terrestrial planet formation during the giant planet
603 instability, and the effect of collisional fragmentation. *Icarus* 321:778–790.
- 604 Cohen B. A., Goodrich C. A., and Keil K. 2004. Feldspathic clast populations in polymict
605 ureilites: Stalking the missing basalts from the ureilite parent body. *Geochimica et*
606 *Cosmochimica Acta* 68:4249–4266.
- 607 Connelly J. N., Bizzarro M., Krot A. N., and Nordlund A. 2012. The absolute chronology and
608 thermal processing of solids in the solar protoplanetary disk. *Science* 338:651–655.
- 609 Connolly H. C., and Jones R. H. 2016. Chondrules: The canonical and noncanonical views.
610 *Journal of Geophysical Research: Planets* 121:1885–1899.
- 611 Crida A., and Charnoz S. 2012. Formation of Regular Satellites from Ancient Massive Rings
612 in the Solar System. *Science* 338:1196–1199.
- 613 Cuzzi J. N., Hogan R. C., and Shariff K. 2008. Toward planetesimals: Dense chondrule
614 clumps in the protoplanetary nebula. *The Astrophysical Journal* 687:1432–1447.
- 615 Daly R. T., and Schultz P. H. 2016. Delivering a projectile component to the vestan regolith.
616 *Icarus* 264:9–19.
- 617 De Sanctis M. C. et al. 2012. Spectroscopic Characterization of Mineralogy and Its Diversity
618 Across Vesta. *Science* 336:697–700.

- 619 Delbo M., Walsh K., Bolin B., Avdellidou C., and Morbidelli A. 2017. Identification of a
620 primordial asteroid family constrains the original planetesimal population. *Science*
621 357:1026–1029.
- 622 Delbo M., Avdellidou C., and Morbidelli A. 2019. Ancient and primordial collisional families
623 as the main sources of X-type asteroids of the inner main belt. *Astronomy &*
624 *Astrophysics* 624:A69.
- 625 DellaGiustina D. N. et al. 2019. Properties of rubble-pile asteroid (101955) Bennu from
626 OSIRIS-REx imaging and thermal analysis. *Nature Astronomy* 3:341–351.
- 627 DellaGiustina D. N. et al. 2020. Variations in color and reflectance on the surface of asteroid
628 (101955) Bennu. *Science* 370:eabc3660.
- 629 DeMeo F. E., and Carry B. 2014. Solar System evolution from compositional mapping of the
630 asteroid belt. *Nature* 505:629–634.
- 631 Dermott S. F., Christou A. A., Li D., Kehoe Thomas. J. J., and Robinson J. M. 2018. The
632 common origin of family and non-family asteroids. *Nature Astronomy* 2:549–554.
- 633 Evatt G. W., Smedley A. R. D., Joy K. H., Hunter L., Tey W. H., Abrahams I. D., and Gerrish
634 L. 2020. The spatial flux of Earth’s meteorite falls found via Antarctic data. *Geology*
635 48:683–687.
- 636 Fujiya W., Sugiura N., Marrocchi Y., Takahata N., Hoppe P., Shirai K., Sano Y., and
637 Hiyagon H. 2015. Comprehensive study of carbon and oxygen isotopic compositions,
638 trace element abundances, and cathodoluminescence intensities of calcite in the
639 Murchison CM chondrite. *Geochim. Cosmochim. Acta* 161:101–117.
- 640 Fujiya W., Hoppe P., Ushikubo T., Fukuda K., Lindgren P., Lee M. R., Koike M., Shirai K.,
641 and Sano Y. 2019. Migration of D-type asteroids from the outer Solar System inferred
642 from carbonate in meteorites. *Nature Astronomy* 3:910–915.
- 643 Gattacceca J., Rochette P., Denise M., Consolmagno G., and Folco L. 2005. An impact origin
644 for the foliation of chondrites. *Earth and Planetary Science Letters* 234:351–368.
- 645 Gattacceca J. et al. 2011. The densest meteorite collection area in hot deserts: The San Juan
646 meteorite field (Atacama Desert, Chile). *Meteoritics & Planetary Science* 46:1276–
647 1287.
- 648 Gattacceca J., Krzesińska A. M., Marrocchi Y., Meier M. M. M., Bourot-Denise M., and
649 Lenssen R. 2017. Young asteroid mixing revealed in ordinary chondrites: The case of
650 NWA 5764, a polymict LL breccia with L clasts. *Meteoritics & Planetary Science*.
651 44:431–16.
- 652 [Goodrich C. A., Hartmann W. K., O’Brien D. P., Weidenschilling S. J., Wilson L., Michel P.,
653 and Jutzi M. 2015. Origin and history of ureilitic material in the solar system: The
654 view from asteroid 2008 TC₃ and the Almahata Sitta meteorite. *Meteoritics &*
655 *Planetary Science* 50:782–809.](#)

- 656 Goodrich C. A. et al. 2019. The first samples from Almahata Sitta showing contacts between
657 ureilitic and chondritic lithologies: Implications for the structure and composition of
658 asteroid 2008 TC₃. *Meteoritics & Planetary Science* 54:2769–2813.
- 659 Gounelle M., Engrand C., Alard O., Bland P. A., Zolensky M. E., RUSSELL S. S., and
660 Duprat J. 2005. Hydrogen isotopic composition of water from fossil micrometeorites
661 in howardites. *Geochimica et Cosmochimica Acta* 69:3431–3443.
- 662 Gounelle M., Spurný P., and Bland P. A. 2006. The orbit and atmospheric trajectory of the
663 Orgueil meteorite from historical records. *Meteoritics & Planetary Science* 41:135–
664 150.
- 665 Gounelle M. 2011. The Asteroid-Comet Continuum: In Search of Lost Primitivity. *Elements*
666 7:29–34.
- 667 Gradie J., and Tedesco E. 1982. Compositional Structure of the Asteroid Belt. *Science*
668 216:1405-1407.
- 669 Greshake A. 2014. A strongly hydrated microclast in the Rumuruti chondrite NWA 6828:
670 Implications for the distribution of hydrous material in the solar system. *Meteoritics &*
671 *Planetary Science* 49:824–841.
- 672 Hanna R. D., Ketcham R. A., Zolensky M., and Behr W. M. 2015. Impact-induced brittle
673 deformation, porosity loss, and aqueous alteration in the Murchison CM chondrite.
674 *Geochimica et Cosmochimica Acta* 171:256–282.
- 675 Hansen B. M. S. 2009. Formation of the terrestrial planets from a narrow annulus.
676 *Astrophysical journal* 703:1131–1140.
- 677 Harvey R. 2003. The Origin and Significance of Antarctic Meteorites. *Geochemistry* 63:93–
678 147.
- 679 Hevey P. J., and Sanders I. S. 2006. A model for planetesimal meltdown by ²⁶Al and its
680 implications for meteorite parent bodies. *Meteoritics & Planetary Science* 41:95–106.
- 681 Hiroi T., Zolensky M.E., and Pieters C.M. 2001. The Tagish Lake Meteorite: A possible
682 Sample from a D-Type Asteroid. *Science* 293:2234-2236.
- 683 Horstmann M. and Bischoff A. (2014). The Almahata Sitta polymict breccia and the late
684 accretion of Asteroid 2008 TC3 - Invited Review. *Chemie der Erde - Geochemistry*
685 74, 149-184.
- 686 Hughes A. M., Duchene G., and Matthews B. 2018. Debris Disks: Structure, Composition,
687 and Variability. *Annual Review of Astronomy and Astrophysics* 56:541–591.
- 688 Huss G. R., Rubin A. E., and Grossman J. N. 2006. Thermal Metamorphism in Chondrites. In
689 Meteorites and the early solar system II, edited by Lauretta D. S. and McSween H. Y.
690 Tucson, Arizona: The University of Arizona Press, pp. 567–586.
- 691 Jaumann R. et al. 2019. Images from the surface of asteroid Ryugu show rocks similar to
692 carbonaceous chondrite meteorites. *Science* 365:817–820.

- 693 Jenniskens P. et al. 2009. The impact and recovery of asteroid 2008 TC3. *Nature* 458:485–
694 488.
- 695 Jenniskens P. et al. 2012. Radar-Enabled Recovery of the Sutter’s Mill Meteorite, a
696 Carbonaceous Chondrite Regolith Breccia. *Science* 338:1583–1587.
- 697 Johansen A., Oishi J. S., Low M.-M. M., Klahr H., Henning T., and Youdin A. 2007. Rapid
698 planetesimal formation in turbulent circumstellar disks. *Nature* 448:1022–1025.
- 699 Johnson B. C., Walsh K. J., Minton D. A., Krot A. N., and Levison H. F. 2016. Timing of the
700 formation and migration of giant planets as constrained by CB chondrites. *Science*
701 *Advances* 2:e1601658.
- 702 Kawasaki N., Park C., Sakamoto N., Park S. Y., Kim H. N., Kuroda M., and Yurimoto H.
703 2019. Variations in initial $^{26}\text{Al}/^{27}\text{Al}$ ratios among fluffy Type A Ca–Al-rich
704 inclusions from reduced CV chondrites. *Earth and Planetary Science Letters* 511:25–
705 35.
- 706 Klahr H., and Schreiber A. 2020. Turbulence Sets the Length Scale for Planetesimal
707 Formation: Local 2D Simulations of Streaming Instability and Planetesimal
708 Formation. *The Astrophysical Journal* 901:54.
- 709 Kööp L., Davis A. M., Nakashima D., Park C., Krot A. N., Nagashima K., Tenner T. J., Heck
710 P. R., and Kita N. T. 2016. A link between oxygen, calcium and titanium isotopes in
711 ^{26}Al -depleted hibonite-rich CAIs from Murchison and implications for the
712 heterogeneity of dust reservoirs in the solar nebula. *Geochimica et Cosmochimica*
713 *Acta* 1–43.
- 714 Lauretta D.S., and McSween H.Y. 2006. Meteorites and the early solar system II. Tucson,
715 Arizona: The University of Arizona Press, 943 p.
- 716 Lauretta D. S. et al. 2019a. The unexpected surface of asteroid (101955) Bennu. *Nature* 1–16.
- 717 Lauretta D. S. et al. 2019b. Episodes of particle ejection from the surface of the active
718 asteroid (101955) Bennu. *Science* 366:eaay3544.
- 719 [Lentfort S., Bischoff A., Ebert S., and Patzek M. 2021: Classification of CM chondrite
720 breccias – implications for the evaluation of samples from the OSIRIS-REx and
721 Hayabusa 2 missions. *Meteoritics & Planetary Science* 56, 127-147.](#)
- 722 Levison H. F., Bottke W. F., Gounelle M., and Morbidelli A. 2009. Contamination of the
723 asteroid belt by primordial trans-Neptunian objects. *Nature* 460:364–366.
- 724 Libourel G., Michel P., Delbo M., Ganino C., Recio-Blanco A., de Laverny P., Zolensky M.
725 E., and Krot A. N. 2017. Search for primitive matter in the Solar System. *Icarus*
726 282:375–379.
- 727 Liu N., Ogliore R. C., and Vacher L. G. 2020. NanoSIMS isotopic investigation of xenolithic
728 carbonaceous clasts from the kapoeta howardite. *Geochimica et Cosmochimica Acta*
729 283:243–264.

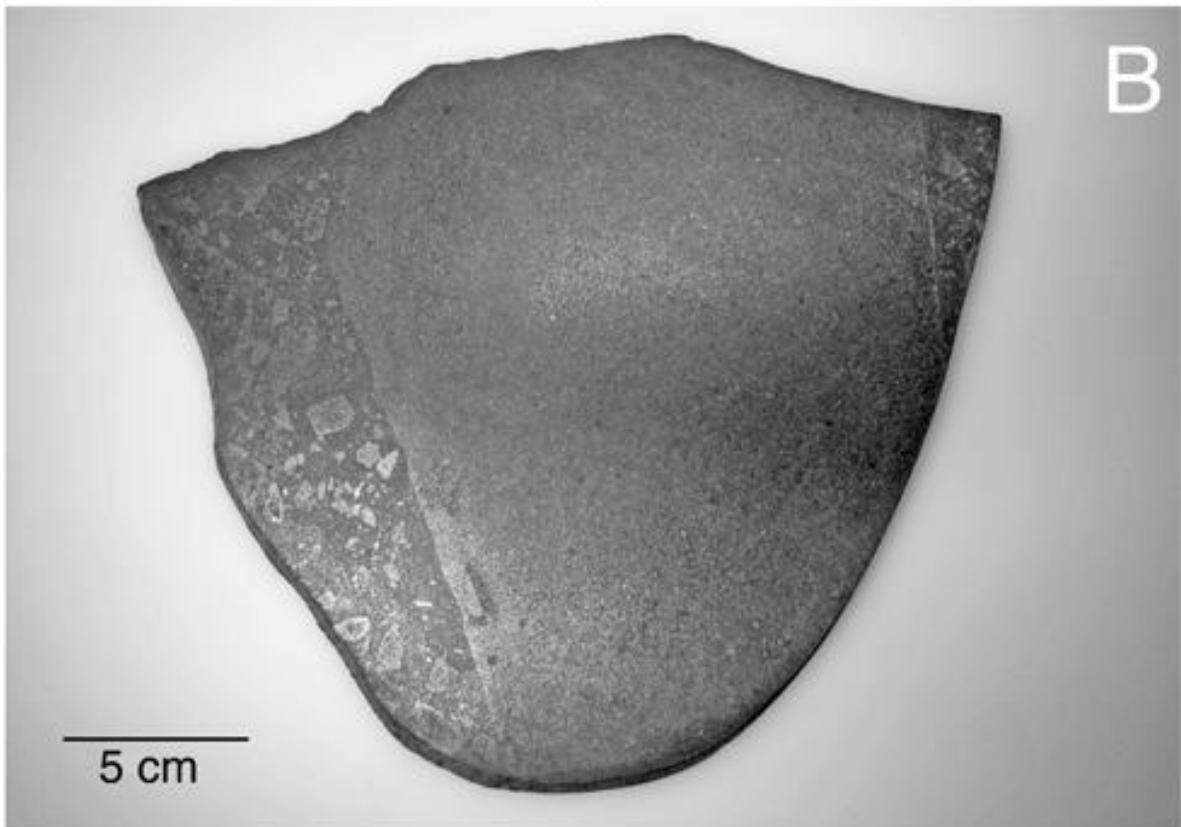
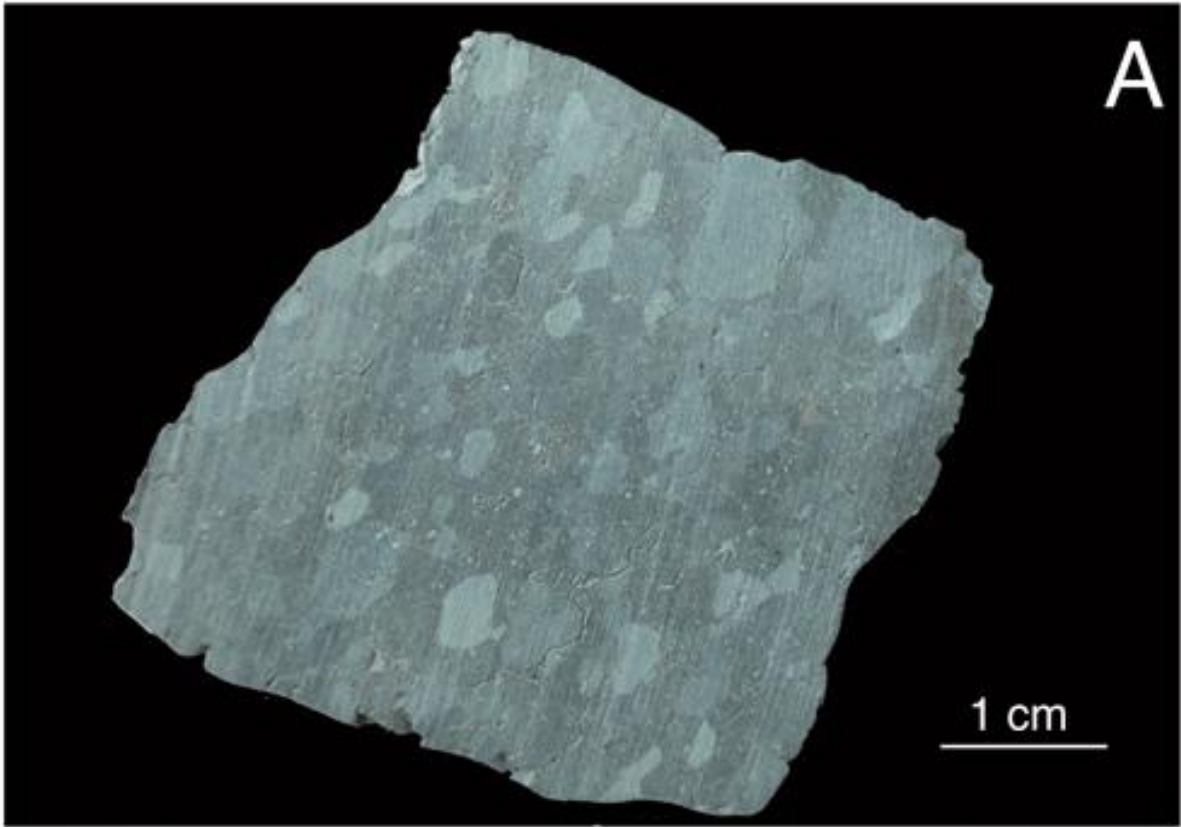
- 730 Lodders K. 2003. Solar system abundances and condensation temperatures of the elements.
731 *The Astrophysical Journal* 591:1220–1247.
- 732 MacPherson G. J., Kita N. T., Ushikubo T., Bullock E. S., and Davis A. M. 2012. Well-
733 resolved variations in the formation ages for Ca–Al-rich inclusions in the early Solar
734 System. *Earth and Planetary Science Letters* 331–332:43–54.
- 735 Marcus A. H. 1967. Formation of the planets by accretion of planetesimals: Some statistical
736 problems. *Icarus* 7:283–296.
- 737 Marrocchi Y., Bekaert D. V., and Piani L. 2018a. Origin and abundance of water in
738 carbonaceous asteroids. *Earth and Planetary Science Letters* 482:23–32.
- 739 Marrocchi Y., Villeneuve J., Batanova V., Piani L., and Jacquet E. 2018b. Oxygen isotopic
740 diversity of chondrule precursors and the nebular origin of chondrules. *Earth and*
741 *Planetary Science Letters* 496:132–141.
- 742 Marrocchi Y., Villeneuve J., Jacquet E., Piralla M., and Chaussidon M. 2019a. Rapid
743 condensation of the first Solar System solids. *Proceedings of the National Academy of*
744 *Sciences of the United States of America* 116:23461–23466.
- 745 Marrocchi Y., Euverte R., Villeneuve J., Batanova V., Welsch B., Ferrière L., and Jacquet E.
746 2019b. Formation of CV chondrules by recycling of amoeboid olivine aggregate-like
747 precursors. *Geochimica et Cosmochimica Acta* 247:121–141.
- 748 Marrocchi Y., and Piani L. 2019. The tumultuous childhood of the Solar System. *Nature*
749 *Astronomy* 889–890.
- 750 Marrocchi Y. et al. 2020. The Piancaldoli meteorite: A forgotten primitive LL3.10 ordinary
751 chondrite. *Meteoritics & Planetary Science* 55:maps.13552.
- 752
- 753 Marrocchi Y., Avice G., and Barrat J.-A. 2021. The Tarda Meteorite: A Window into the
754 Formation of D-type Asteroids. *The Astrophysical Journal Letters* 913:L9.
- 755
- 756 Marsset M. et al. 2020. The violent collisional history of aqueously evolved (2) Pallas. *Nature*
757 *Astronomy* 4:569–576.
- 758 Masiero J. R., Grav T., Mainzer A. K., Nugent C. R., Bauer J. M., Stevenson R., and Sonnett
759 S. 2014. Main-belt asteroids with *wise* /neowise: near-infrared albedos. *The*
760 *Astrophysical Journal* 791:121.
- 761 McCord T. B. et al. 2012. Dark material on Vesta from the infall of carbonaceous volatile-
762 rich material. *Nature* 491:83–86.
- 763 McSween H. Y., Mittlefehldt D. W., Beck A. W., Mayne R. G., and McCoy T. J. 2011. HED
764 Meteorites and Their Relationship to the Geology of Vesta and the Dawn Mission.
765 *Space Science Reviews* 163:141–174.
- 766 Michel P. 2001. Collisions and Gravitational Reaccumulation: Forming Asteroid Families and
767 Satellites. *Science* 294:1696–1700.

- 768 Michel P., and Richardson D. C. 2013. Collision and gravitational reaccumulation: Possible
769 formation mechanism of the asteroid Itokawa. *Astronomy & Astrophysics* 554:L1.
- 770 Michel P. et al. 2020. Collisional formation of top-shaped asteroids and implications for the
771 origins of Ryugu and Bennu. *Nature Communications* 11:2655.
- 772 Minton D. A., and Malhotra R. 2009. A record of planet migration in the main asteroid belt.
773 *Nature* 457:1109–1111.
- 774 Morbidelli A., Bottke W., Nesvorný D., and Levison H. F. 2009. Asteroids Were Born Big.
775 *Icarus* 204:558–573.
- 776 Morbidelli A., Brassier R., Gomes R., Levison H. F., and Tsiganis K. 2010. Evidence from the
777 asteroid belt for a violent past evolution of Jupiter's orbit. *The Astronomical Journal*
778 140:1391–1401.
- 779 Morbidelli A., Bitsch B., Crida A., Gounelle M., Guillot T., Jacobson S., Johansen A.,
780 Lambrechts M., and Lega E. 2016. Fossilized condensation lines in the Solar System
781 protoplanetary disk. *Icarus* 267:368–376.
- 782 Morbidelli A., and Raymond S. N. 2016. Challenges in planet formation: Challenges in planet
783 formation. *Journal of Geophysical Research: Planets* 121:1962–1980.
- 784 Morlok A., Bischoff A., Stephan T., Floss C., Zinner E., and Jessberger E. K. 2006.
785 Brecciation and chemical heterogeneities of CI chondrites. *Geochimica et*
786 *Cosmochimica Acta* 70:5371–5394.
- 787 Nesvorný D., Broz M., and Carruba V. 2015. Identification and Dynamical Properties of
788 Asteroids IV, Patrick Michel, Francesca E. DeMeo, and William F. Bottke (eds.),
789 University of Arizona Press, Tucson, pp. 297-321.
- 790 O'Brien D. P., and Sykes M. V. 2011. The origin and evolution of the asteroid belt—
791 Implications for Vesta and Ceres. *Space science reviews* 163:41–61.
- 792 Okada T. et al. 2020. Highly porous nature of a primitive asteroid revealed by thermal
793 imaging. *Nature* 579:518–522.
- 794 Pape J., Mezger K., Bouvier A.-S., and Baumgartner L. P. 2019. Time and duration of
795 chondrule formation: Constraints from ^{26}Al - ^{26}Mg ages of individual chondrules.
796 *Geochimica et Cosmochimica Acta* 244:416–436.
- 797 Patzek M., Bischoff A., Visser R., and John T. 2018. Mineralogy of volatile-rich clasts in
798 brecciated meteorites. *Meteoritics & Planetary Science* 43:435–22.
- 799 Patzek M., Hoppe P., Bischoff A., Visser R., and John T. 2020. Hydrogen isotopic
800 composition of CI- and CM-like clasts from meteorite breccias – Sampling unknown
801 sources of carbonaceous chondrite materials. *Geochimica et Cosmochimica Acta*
802 272:177–197.
- 803 Petitat M., Marrocchi Y., McKeegan K. D., Mostefaoui S., Meibom A., Zolensky M. E., and
804 Gounelle M. 2011. ^{53}Mn - ^{53}Cr ages of Kaidun carbonates. *Meteoritics & Planetary*
805 *Science* 46:275–283.

- 806 Piani L., Marrocchi Y., Libourel G., and Tissandier L. 2016. Magmatic sulfides in the
807 porphyritic chondrules of EH enstatite chondrites. *Geochimica et Cosmochimica Acta*
808 195:84–99.
- 809 Piani L., Marrocchi Y., Rigaudier T., Vacher L. G., Thomassin D., and Marty B. 2020.
810 Earth's water may have been inherited from material similar to enstatite chondrite
811 meteorites. *Science* 369:1110–113.
- 812 Piani L., Marrocchi Y., Vacher L. G., Yurimoto H., and Bizzarro M. 2021. Origin of
813 hydrogen isotopic variations in chondritic water and organics. *Earth and Planetary*
814 *Science Letters* 567:117008.
- 815 Raymond S.N, Mandell A.M., Sigrudsson S. 2006. Exotic Earths: Forming Habitable Worlds
816 with Giant Planet Migration. *Science* 313:1413-1416.
- 817 Raymond S. N., O'Brien D. P., Morbidelli A., and Kaib N. A. 2009. Building the terrestrial
818 planets: Constrained accretion in the inner solar system. *Icarus* 203:644–662.
- 819 Raymond S. N., and Izidoro A. 2017a. Origin of water in the inner Solar System:
820 Planetesimals scattered inward during Jupiter and Saturn's rapid gas accretion. *Icarus*
821 297:134-148.
- 822 Raymond S. N., and Izidoro A. 2017b. The empty primordial asteroid belt. *Science Advances*
823 3:e1701138.
- 824 Raymond S. N., and Morbidelli A. 2020. Planet formation: key mechanisms and global
825 models. *arXiv:2002.05756*.
- 826 Rubin A. E. 1983. The Adhi Kot breccia and implications for the origin of chondrules and
827 silica-rich clasts in enstatite chondrites. *Earth and Planetary Science Letters* 64:201–
828 212.
- 829 Rubin A. E., and Bottke W. F. 2009. On the origin of shocked and unshocked CM clasts in H-
830 chondrite regolith breccias. *Meteoritics & Planetary Science* 44:701–724.
- 831 Rubin A. E. 2012. Collisional facilitation of aqueous alteration of CM and CV carbonaceous
832 chondrites. *Geochimica et Cosmochimica Acta* 90:181–194.
- 833 [Rubin A. E. 2015. Impact features of enstatite-rich meteorites. *Geochemistry* 75:1–28.](#)
- 834 Safronov V. S., and Zvjagina E. V. 1969. Relative sizes of the largest bodies during the
835 accumulation of planets. *Icarus* 10:109–115.
- 836 Sahijpal S., Soni P., and Gupta G. 2007. Numerical simulations of the differentiation of
837 accreting planetesimals with ²⁶Al and ⁶⁰Fe as the heat sources. *Meteoritics &*
838 *Planetary Science* 42:1529–1548.
- 839 Schenk P. et al. 2012. The Geologically Recent Giant Impact Basins at Vesta's South Pole.
840 *Science* 336:694–697.

- 841 Schlüter J., Schultz L., Thiedig F., Al-Mahdi B.O., and Abu Aghreb A.E. 2002. The Dar al
842 Gani meteorite field (Libyan Sahara): Geological setting, pairing of meteorites, and
843 recovery density. *Meteoritics & Planetary Science*. 37:1070–1093.
- 844 Sharp T.G., and DeCarli P.S. 2006. Shock Effects in Meteorites. In Meteorites and the early
845 solar system II, edited by Lauretta D. S. and McSween H. Y. Tucson, Arizona: The
846 University of Arizona Press. pp. 653-677.
- 847 Stöffler, D., Hamann, C., & Metzler, K. 2018. Shock metamorphism of planetary silicate
848 rocks and sediments: Proposal for an updated classification system. *Meteoritics &
849 Planetary Science* 53:5-49.
- 850 Stooke P.J. 1996. The Surface of Asteroid 951 Gaspra. *Earth, Moon and Planets* 75:53-75.
- 851 Sugita S. et al. 2019. The geomorphology, color, and thermal properties of Ryugu:
852 Implications for parent-body processes. *Science* 364:252.
- 853 Suttle, M. D., King, A. J., Schofield, P. F., Bates, H., & Russell, S. S. 2021. The aqueous
854 alteration of CM chondrites, a review. *Geochimica et Cosmochimica Acta* 299:219-
855 256.
- 856 Tatsumi E. et al. 2021. Collisional history of Ryugu's parent body from bright surface
857 boulders. *Nature astronomy* 5:39-45.
- 858 Terada K. and Bischoff A. 2009. Asteroidal granite-like magmatism 4.53 Gyr ago. *The
859 Astrophysical Journal* 699, L68-L71.
- 860 Thomas P. C., Binzel R. P., Gaffey M. J., Storrs A. D., Wells E. N., and Zellner B. H. 1997.
861 Impact Excavation on Asteroid 4 Vesta: Hubble Space Telescope Results. *Science*
862 277:1492–1495.
- 863 Tsiganis K., Gomes R., Morbidelli A., and Levison H. F. 2005. Origin of the orbital
864 architecture of the giant planets of the Solar System. *Nature* 435:459–461.
- 865 Tsirvoulis G., Morbidelli A., Delbo M., and Tsiganis K. 2018. Reconstructing the size
866 distribution of the primordial Main Belt. *Icarus* 304:14–23.
- 867 Turner S., McGee L., Humayun M., Creech J., and Zanda B. 2021. Carbonaceous chondrite
868 meteorites experienced fluid flow within the past million years. *Science* 371:164–167.
- 869 Turrini D., Svetsov V., Consolmagno G., Sirono S., and Pirani S. 2016. Olivine on Vesta as
870 exogenous contaminants brought by impacts: Constraints from modeling Vesta's
871 collisional history and from impact simulations. *Icarus* 280:328–339.
- 872 Vacher L. G., Marrocchi Y., Villeneuve J., Verdier-Paoletti M. J., and Gounelle M. 2017.
873 Petrographic and C & O isotopic characteristics of the earliest stages of aqueous
874 alteration of CM chondrites. *Geochimica et Cosmochimica Acta* 213:271–290.
- 875 Vacher L. G., Marrocchi Y., Villeneuve J., Verdier-Paoletti M. J., and Gounelle M. 2018.
876 Collisional and alteration history of the CM parent body. *Geochimica et
877 Cosmochimica Acta* 239:213–234.

- 878 Vacher L. G., Truche L., Faure F., Tissandier L., Mosser-Ruck R., and Marrocchi Y. 2019a.
879 Deciphering the conditions of tochilinite and cronstedtite formation in CM chondrites
880 from low temperature hydrothermal experiments. *Meteoritics & Planetary Science*.
881 54:1870–1889.
- 882 Vacher L. G., Piralla M., Gounelle M., Bizzarro M., and Marrocchi Y. 2019b. Thermal
883 Evolution of Hydrated Asteroids Inferred from Oxygen Isotopes. *The Astrophysical*
884 *Journal Letters* 882:0–0.
- 885 Vacher L. G., Piani L., Rigaudier T., Thomassin D., Florin G., Piralla M., and Marrocchi Y.
886 2020. Hydrogen in chondrites: Influence of parent body alteration and atmospheric
887 contamination on primordial components. *Geochimica et Cosmochimica Acta* 281:53–
888 66.
- 889 [van Drongelen K. D., Rumble III D. and Tait K. T. 2016. Petrology and oxygen isotopic
890 compositions of clasts in HED polymict breccia NWA 5232. *Meteoritics & Planetary*
891 *Science* 51:1184-1200.](#)
- 892 van Schmus W.R., and Wood J.A. 1967. A chemical-petrologic classification for the
893 chondritic meteorites. *Geochimica et Cosmochimica Acta* 31:747–765.
- 894 Verdier-Paoletti M. J., Marrocchi Y., Vacher L. G., Gattacceca J., Gurenko A., Sonzogni C.,
895 and Gounelle M. 2019. Testing the genetic relationship between fluid alteration and
896 brecciation in CMchondrites. *Meteoritics & Planetary Science* 54:395–18.
- 897 Veverka J., Belton M., Klaasen K., and Chapman C. 1994. Galileo's Encounter with 951
898 Gaspra: Overview. *Icarus* 107:2-17.
- 899 Villeneuve J., Chaussidon M., and Libourel G. 2009. Homogeneous Distribution of ²⁶Al in
900 the Solar System from the Mg Isotopic Composition of Chondrules. *Science* 325:985–
901 988.
- 902 Walsh K. J., Morbidelli A., Raymond S. N., O'Brien D. P., and Mandell A. M. 2011. A low
903 mass for Mars from Jupiter's early gas-driven migration. *Nature* 475:206–209.
- 904 Walsh K. J. et al. 2019. Craters, boulders and regolith of (101955) Bennu indicative of an old
905 and dynamic surface. *Nature Geoscience* 12:242–246.
- 906 Wetherill G. W. 1990. Formation of the Earth. *Annual Review of Earth and Planetary*
907 *Sciences* 18:205–256.
- 908 Wurm G., Paraskov G., and Krauss O. 2005. Growth of planetesimals by impacts at ~25 m/s.
909 *Icarus* 178:253–263.
- 910 Zolensky M. E., Ivanov A. V., Yang S. V., Mittlefehldt D. W., and Ohsumi K. 1996. The
911 Kaidun meteorite: Mineralogy of an unusual CM1 lithology. *Meteoritics & Planetary*
912 *Science* 31:484–493.
- 913 Zolensky M., and Ivanov A. 2003. The Kaidun Microbreccia Meteorite: A Harvest from the
914 Inner and Outer Asteroid Belt. *Chemie der Erde - Geochemistry* 63:185–246.
- 915

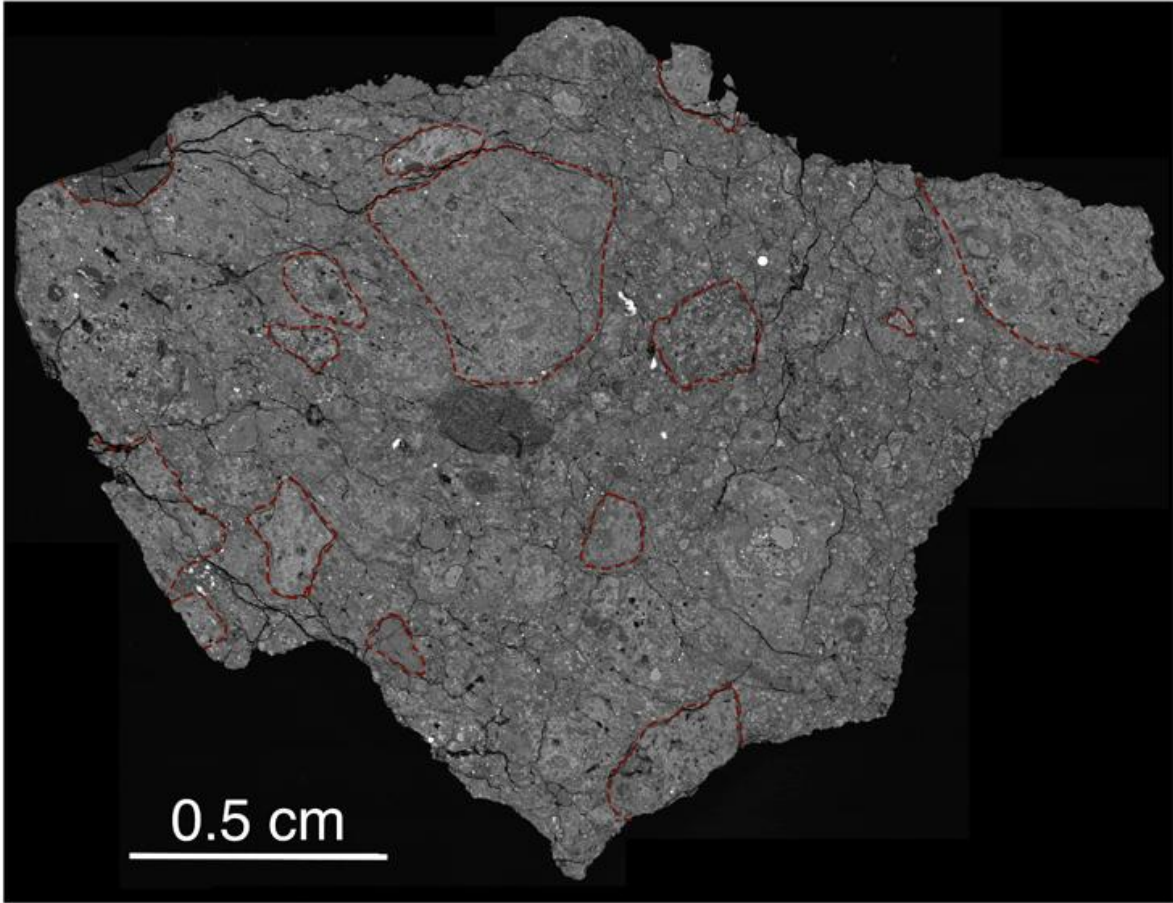


916

917

918

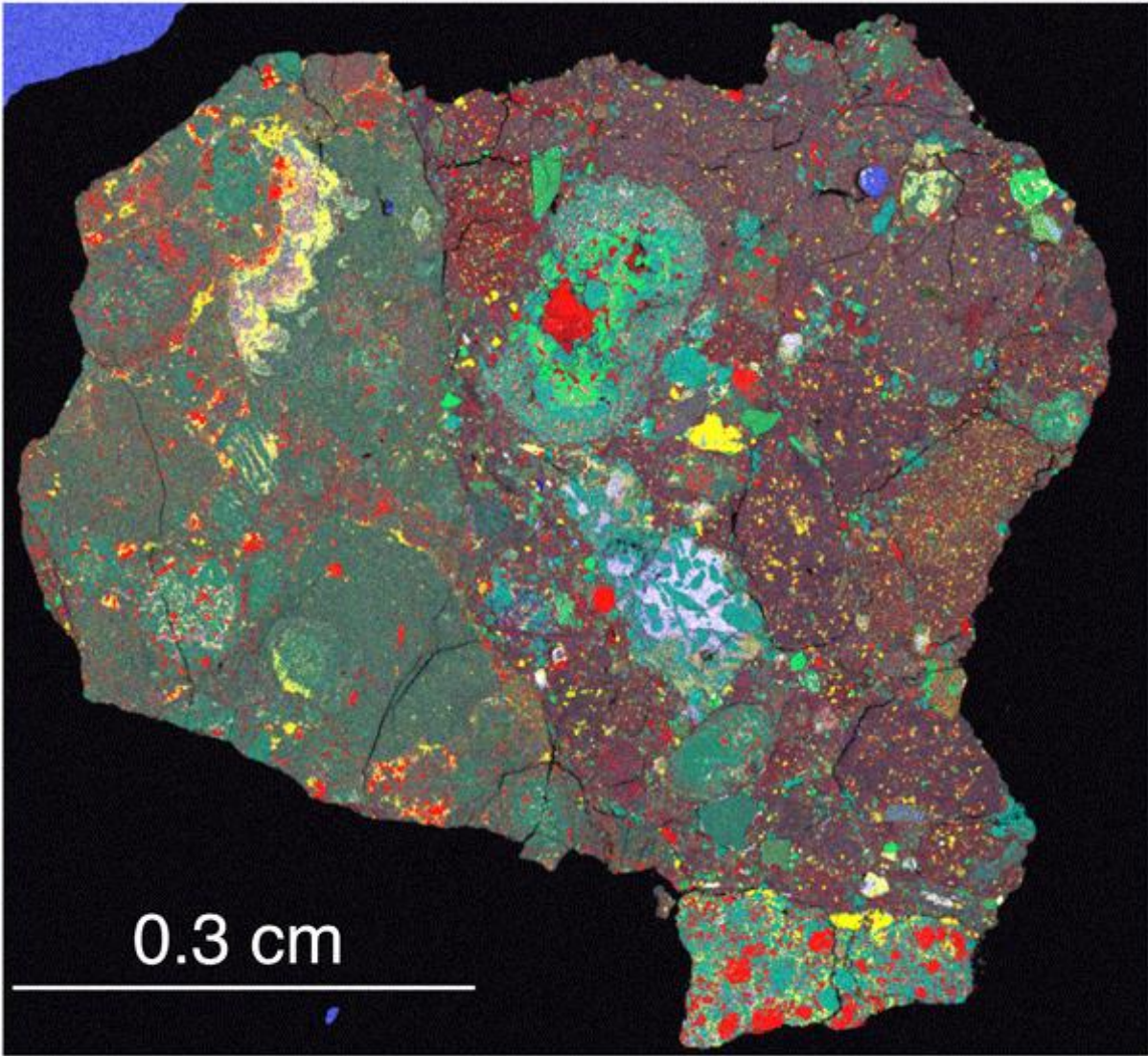
Fig. 1



919

920

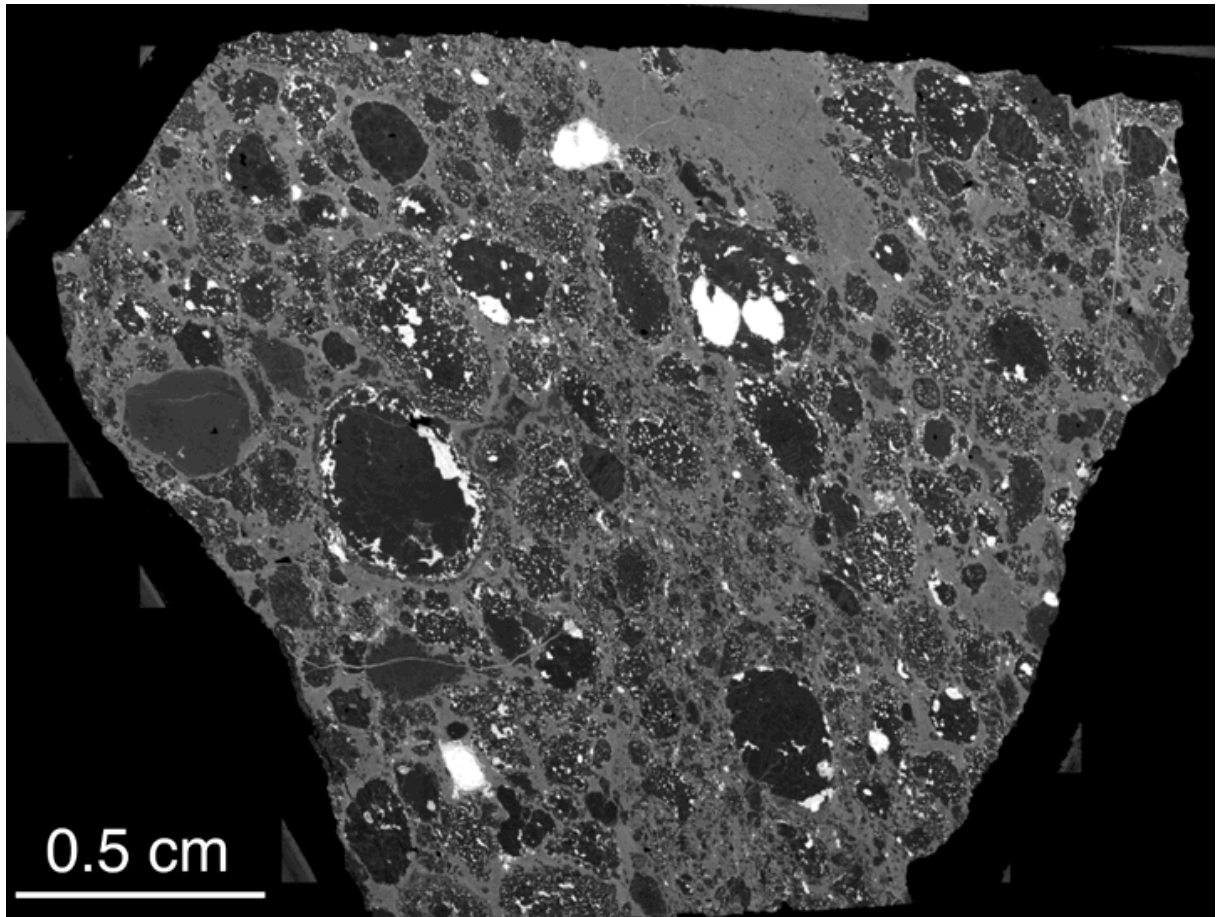
Fig. 2



921

922

Fig. 3

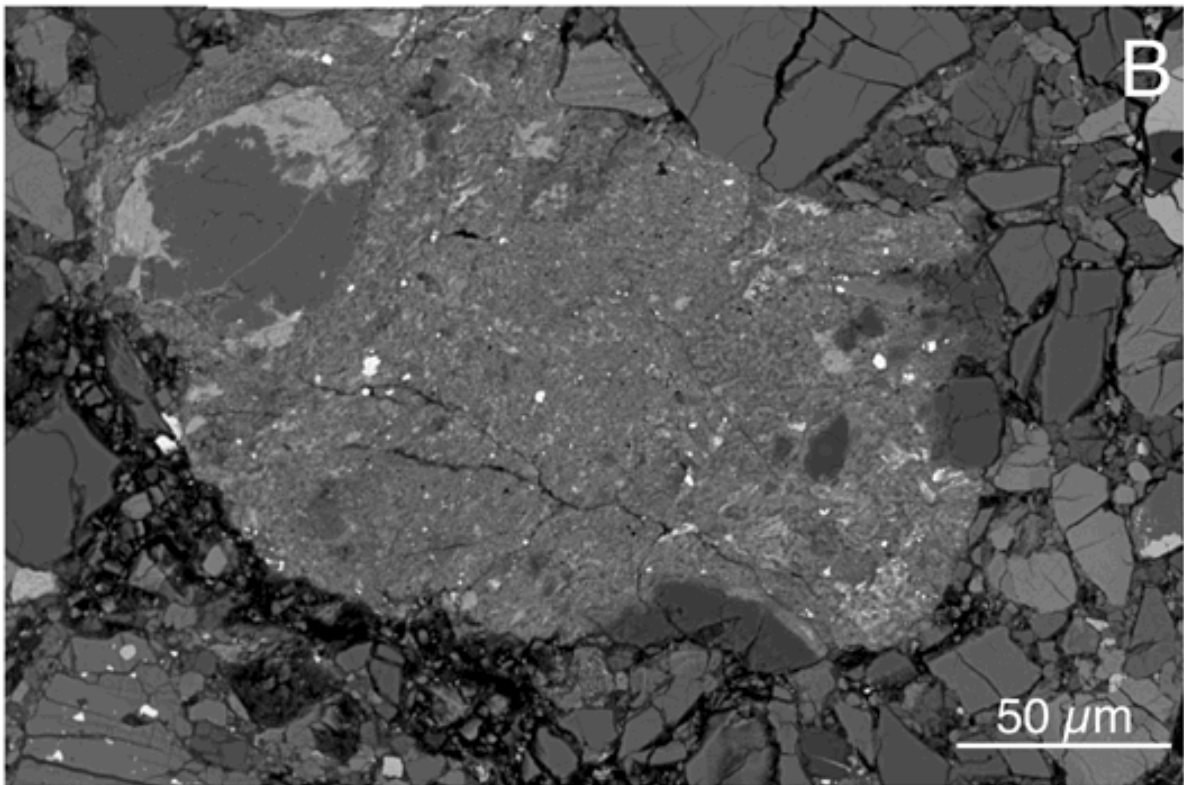
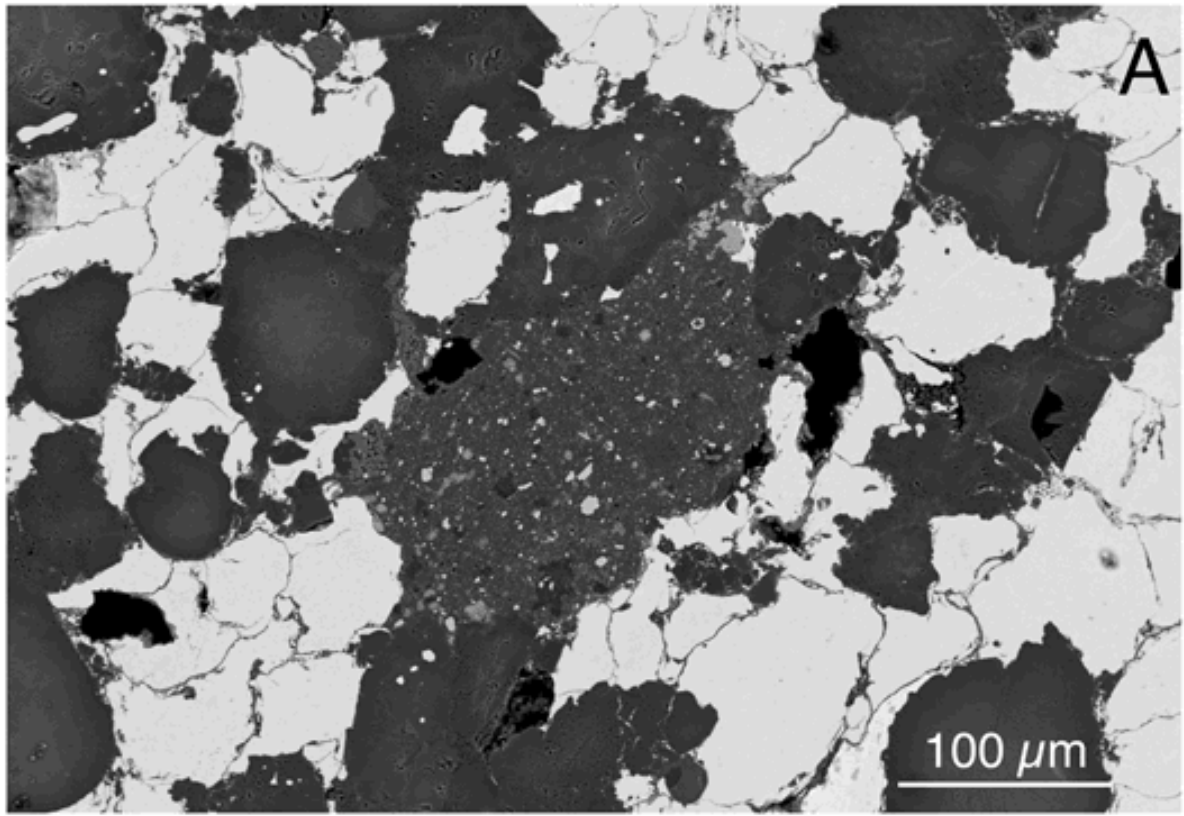


923

924

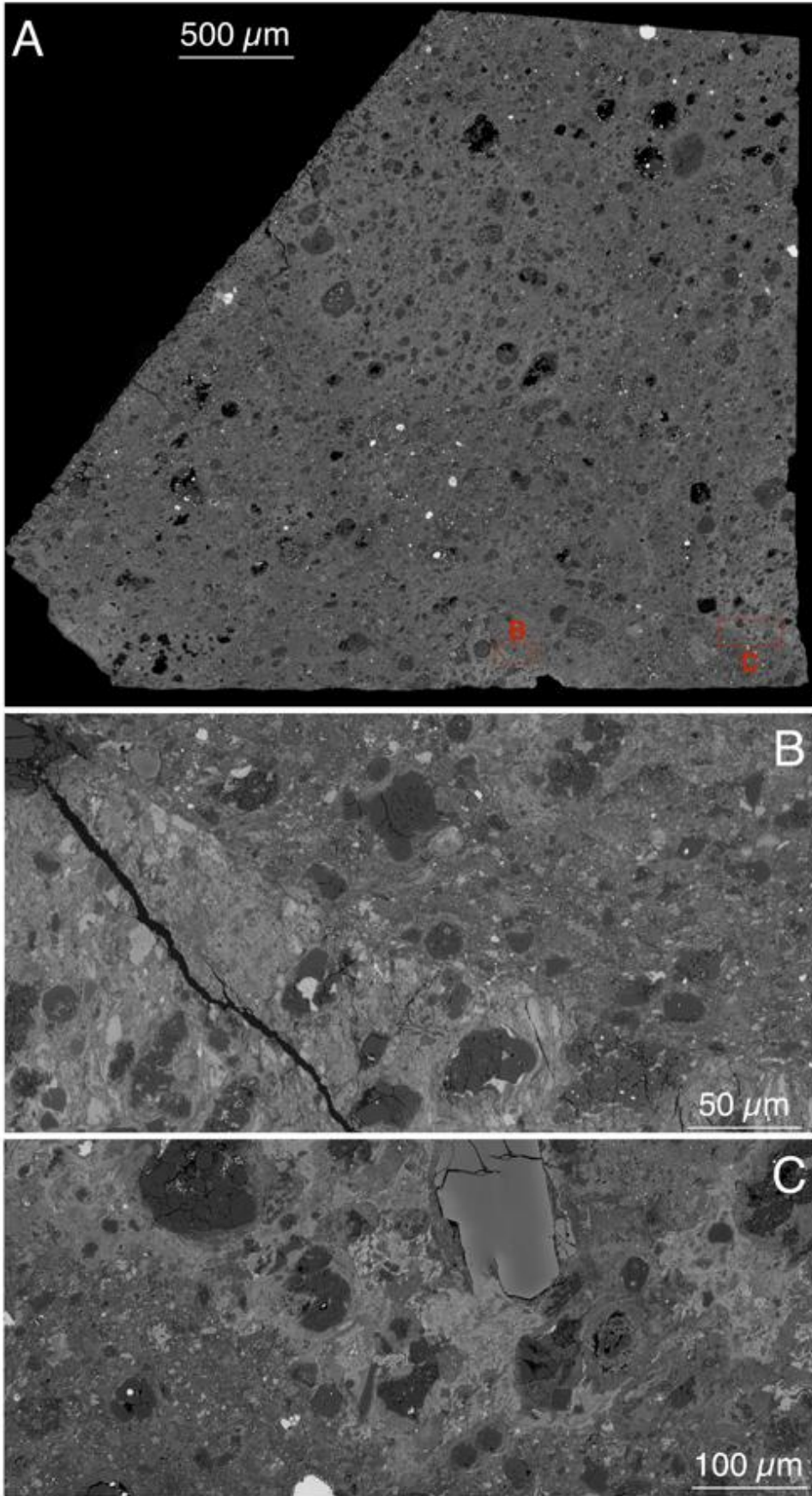
925

Fig. 4



926
927
928
929

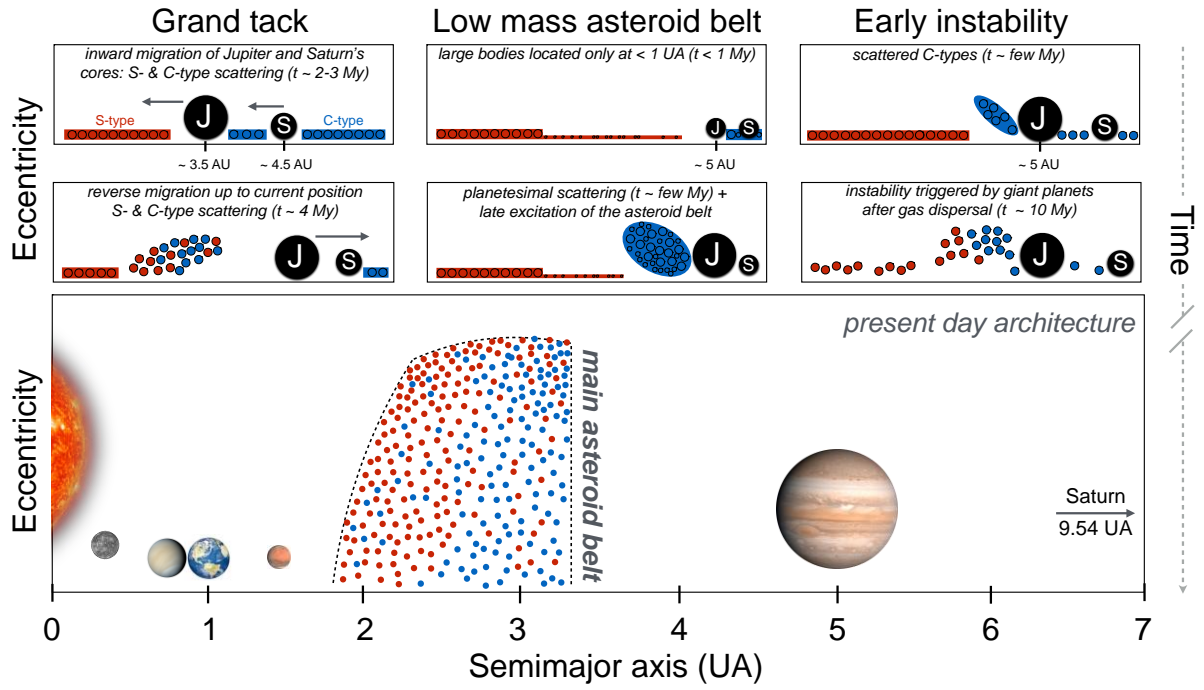
Fig. 5



930

931

Fig. 6



932

933

934

935

936

Fig. 7